PASSIVE FORCE-DEFLECTION CURVES FOR SKEWED ABUTMENTS

Kyle M. Rollins[1] and Shon J. Jessee[2]

ABSTRACT: The passive force-deflection relationship for abutment walls is important for bridges subjected to thermal expansion and seismic forces, but no test results have been available for skewed abutments. To determine the influence of skew angle on the development of passive force, lab tests were performed on a wall with skew angles of 0º, 15º, 30º, and 45º. The wall was 1.26 m wide and 0.61 m high and the backfill consisted of dense compacted sand. As the skew angle increased, the passive force decreased substantially with a reduction of 50% at a skew of 30º. An adjustment factor was developed to account for the reduced capacity as a function of skew angle. The shape of the passive force-deflection curve leading to the peak force transitioned from a hyperbolic shape to a more bilinear shape as the skew angle increased. However, the horizontal displacement necessary to develop the peak passive force was still between 2 to 4% of the wall height. In all cases, the passive force decreased after the peak value, which would be expected for dense sand; however, at higher skew angles the drop in resistance was more abrupt. The residual passive force was typically 40% lower than the peak force. For nearly all skew angles, the transverse shear resistance exceeded the applied shear force on the wall so that transverse movement was minimal. Computer models using the plane strain friction angle were able to match the measured force for the no skew case as well as for skewed cases when the proposed adjustment factor was used.

Keywords: Bridge abutments**,** Integral abutments, Passive pressure, Skewed abutments, Skewed Bridges, Sand, Seismic Design

[1] Prof. Civ. & Env. Engrg. Dept., Brigham Young Univ., 368 CB, Provo, UT 84602, rollinsk@byu.edu
[2] Staff Engr., Terracon Consultants, Inc., 5301 Beverly Dr., Oklahoma City, OK 73013, sjjess@gmail.com

INTRODUCTION

Over the past 20 years a number of large scale tests have been performed to define the passive force-deflection curve which might be expected for dense compacted fill behind bridge abutments (Maroney 1995, Mokwa and Duncan 2001, Rollins and Cole 2006, Rollins and Sparks 2002, Lemnitzer et al 2009). These tests have generally shown that the ultimate passive force is best approximated using the log spiral approach and that the maximum force requires a deflection equal to 3 to 5% of the wall height (Rollins and Cole 2006). The complete passive force-deflection curve can best be estimated by a hyperbolic curve using techniques described by Shamsabadi et al. (2007) or by Duncan and Mokwa (2001); however, for simplicity design guidelines often recommend a bilinear relationship (Caltrans 2001, AASHTO 2011).

Although these findings are clearly useful in bridge engineering design, there is considerable uncertainty about their applicability for skewed abutments where the passive force develops at an angle relative to the longitudinal axis of the bridge structure as shown in Fig. 1. This becomes particularly important in light of the fact that about 41% of 605,000 bridges in the US bridge database are skewed (Nichols, personal communication, 2012). While current design codes (AASHTO 2011) consider that the ultimate passive force will be the same for a skewed abutment as for a non-skewed abutment, numerical analyses performed by Shamsabadi et al. (2006) indicate that the passive force will decrease substantially as the skew angle increases. Reduced passive force on skewed abutments would be particularly important for bridges subject to seismic forces or integral abutments subject to thermal expansion. In fact, some field evidence indicates poorer performance of skewed abutments during seismic events (Shamsabadi et al 2006, Unjohn 2012, Apirakvorapinit et al 2012, Elnashai et al, 2010) and distress to skewed abutments due to thermal expansion (Steinberg and Sargand 2010). Unfortunately, there have not been any physical passive force test results for skewed abutments reported in the literature which could guide engineers in making appropriate adjustments for skewed conditions.

To understand better the influence of skew angle on the development of passive force, a series of large size laboratory tests were performed on a wall that was 1.26 m (4.1 ft) wide and 0.61 m (2 ft) high. A dense sand was compacted behind the wall to simulate a bridge approach fill. Passive force-deflection curves were measured for skew angles of 0º, 15º, 30º, and 45º. This paper describes the test program, the test results, and the implications for design practice based on analysis of the test results.

BACKGROUND

The distribution of forces at the interface between a skewed bridge and the adjacent backfill soil is illustrated in Fig. 1 as originally outlined by Burke (1994). The longitudinal force (P_L) can be induced by thermal expansion or seismic forces. For static or simplified pseudo-static analyses, the components of the longitudinal force normal and transverse to the abutment must be resisted by the passive force (P_p) normal to the abutment backwall and the shear resistance (P_R) on the backwall. Summing forces normal to the abutment produces the equation

$$P_p = P_L \cos\theta \quad (1)$$

where θ is the skew angle of the backwall.

The transverse applied shear force (P_T) can be computed using the equation

$$P_T = P_L \sin\theta \quad (2)$$

While the transverse shear resistance (P_R) can be given by the equation

$$P_R = cA + P_p \tan\delta \quad (3)$$

Summing forces transverse to the backwall produces the equation

$$(cA + P_p \tan\delta)/F_s \geq P_L \sin\theta \quad (4)$$

where c is the soil cohesion, A is the area of the backwall, δ is the angle of wall friction between the backfill soil and the concrete abutment backwall, and F_s is a factor of safety. If the applied transverse shear resistance exceeds the ultimate shear resistance, the abutment could slide against the soil leading to an unstable condition.

In addition, the offset in passive force on the abutments produce a force couple which must be resisted by the force couple produced by the shear resistances on each abutment. Summing moments about a vertical axis leads to the equation

$$(cA + P_p \tan\delta)\, L \cos\theta/F_s \geq P_p\, L \sin\theta \quad (5)$$

Again, if the shear resistance is insufficient, the bridge will tend to rotate, which would likely change the distribution of passive force on the abutments. Based on Eq 5, Burke (1994) suggested that rotation would be expected for skew angles greater than 15º with smooth abutment-soil interfaces and no cohesion as the factor of safety dropped from 1.5 to 1.0. If cohesion is ignored, the potential for rotation is independent of both P_p and the length of the bridge, L.

TEST LAYOUT

To understand better the influence of skew angle on the development of passive force, a series of laboratory tests were performed. A plan view of the test layout is provided in Fig. 2. A concrete wall 1.26 m (4.13 ft) wide and 0.61 m (2 ft) high was used to model the backwall of an abutment. Passive force-deflection tests were performed with skew angles (θ) of 0º, 15º, 30º, and 45º. Two tests were performed for each skew angle to evaluate repeatability. A dense sand was compacted behind the wall to simulate the backfill in a typical approach fill. The sand backfill was 0.9 m (3 ft) thick and extended 0.3 m (1 ft) below the base of the wall to allow a potential failure surface to develop below the wall as might be expected for a log-spiral failure geometry. The backfill was 3 to 4 m (10 to 13 ft) long to completely contain the failure surface and was slightly wider than the wall 1.28 m (4.21 ft) to allow the backwall to move into the sand backfill without any friction on the concrete sidewall. To support the sand backfill during compaction, two 1. 5 m concrete blocks were bolted to the structural floor of the laboratory on either side of the fill near the wall. Beyond the concrete blocks, plywood walls were braced into a vertical position. Two plastic sheets were placed along the sidewalls of the backfill to create a low friction surface and produce a 2D or approximately plane strain geometry. A base was constructed below the concrete backwall and rollers were placed at the interface between the backwall and the base to provide a normal force but minimize base friction.

Tests were performed by pushing the backwall longitudinally into the backfill sand using a 490 kN (110 kip) hydraulic actuator which was bolted to the backwall. Load was applied at a rate of 0.25 mm/min (0.1 inch/min). Vertical and horizontal load cells were mounted between the reaction frame and the actuator so that the loads necessary to hold the wall in place could be measured. Nevertheless, because of the flexibility of the actuator piston, there was still a small amount of movement of the backwall at the soil-wall interface.

Instrumentation

Load was measured by pressure transducers in the actuator. To measure the movement of the backwall, four longitudinal string potentiometers were positioned at the corners of the wall and two transverse string pots were positioned at the top and bottom of one side. In addition, a final string pot was used to monitor the vertical movement. Longitudinal string pots were also attached to steel rods driven into the backfill surface at distances of approximately 0.6, 1.2 and

1.8 m (2, 4 and 6 ft) behind the backwall to determine average compressive strain within the backfill soil. All string potentiometers were connected to an independent reference frame.

To help identify the position of the failure surface on the ground, 0.3 m (1 ft) square grids were marked on the surface of the backfill. The change in elevation of the centerline of the backfill was also measured at each grid point with a survey level. To locate the failure surface within the backfill, a hand auger was used to drill 50 mm (2 inch) diameter vertical holes through the backfill at a series of locations behind the backwall. These holes were then backfilled and compacted with red sand. At the conclusion of each test, a longitudinal trench was excavated and the offset in the red sand column provided the location of the failure surface with distance from the wall face.

Geotechnical Properties of the Backfill

The sand backfill is clean poorly-graded sand classifying as SP according to the Unified Soil Classification System and A-1-b according to the AASHTO system. The particle size distribution curve falls within the gradation limits for washed concrete sand (ASTM C33) as shown in Fig. 3 with C_u of 3.7 and C_c of 0.7.

Unit weight and Moisture Content

A modified Proctor test was performed on the sand and indicated a maximum dry unit weight of 17.8 kN/m^3 (113.5 lbs/ft^3). Although the optimum moisture content was 13% the curve was not highly sensitive to moisture content. The sand was compacted into the box with a jumping jack compactor in 150 mm (6 inch) lifts to achieve an average relative compaction greater than 95% as specified by many design standards. A typical histogram of relative compaction based on nuclear density test results is provided in Fig. 4 and a summary of the mean relative compaction and water content at the time of each test is provided in Table 1. Typically, the average relative compaction was about 98% with a moisture content of 8%. Based on a correlation developed by Lee and Singh (1971), the relative density (D_r) for this level of compaction would be about 90%.

Load testing was generally performed two days after compaction and moisture content measurements were made immediately after testing. The moisture content as a function of depth for the various tests is shown in Fig. 5. The moisture content curves for the various tests generally fall within one or two percent of one another indicating good consistency between tests.

Shear strength

Based on a direct shear test on the sand compacted at the density and moisture content in the sand box, the drained friction angle (ϕ') was found to be 46º with a cohesion of 7 kPa (140 psf). Shear stress versus horizontal displacement curves typically showed a 35 to 40% reduction in shear strength from the peak to the residual value with a residual friction angle of 33º. Interface friction tests were also performed between the sand and the concrete and a wall friction angle (δ) of 33º was measured. Therefore, the δ/ϕ is 0.72 which is in good agreement with results from other researchers (Potyondy, 1961, Cole and Rollins, 2006).

Because the compacted sand in a partially saturated state could be excavated with a vertical face and remained stable for long periods, the potential for apparent cohesion owing to matric suction was also investigated. Suction measurements indicated that the sand at the moisture content during testing had a matric suction (ψ) (negative pressure relative to atmospheric pressure) of approximately 4 to 5 kPa (80 to 100 psf). At this water content the degree of saturation (S) was between 40 and 50%. Based on the recommendations of Likos et al (2010), the apparent cohesion (c_a) for the partially saturated sand can be given by the equation,

$$c_a = S_e \, \psi \tan\phi' \tag{6}$$

where the effective saturation (S_e) as a fraction is given by the equation

$$S_e = (S - S_r)/(1 - S_r) \tag{7}$$

and S_r is the residual or lower bound saturation at high matric suctions. S_r is obtained from a water retention curve which defines the relationship between saturation and matric suction. A water retention curve for the sand was determined using a porous pressure plate apparatus and indicated that S_r is 14%. For the conditions during the passive force testing, the apparent cohesion determined from Eq. 6 would be approximately 4 to 5 kPa (80 to 100 psf).

TEST RESULTS

Passive Force-Deflection Curves

The passive force versus longitudinal deflection curves for the tests at each of the skew angles are plotted in Fig. 6. The passive force was computed from the applied actuator force using Eq. 1 while the wall deflection was the average of the four longitudinal strain potentiometers. Generally, the results from the pair of tests at each skew angle were reasonably consistent; however, some variations are apparent for post-peak response. Although the initial stiffness for each curve is remarkably similar, the peak passive force clearly decreases as the skew angle increases.

While the passive force-deflection curve appears to exhibit a typical hyperbolic curve shape for the no skew case, it transitions to a different shape as the skew angle increases. As the skew angle increases, the passive force exhibits a longer plateau where the force remains relatively constant or increases gradually with deflection before reaching a peak and abruptly decreasing to a residual value. The peak passive force typically developed at a normalized deflection of 2.5% to 3.5% of the wall height (H), and did not change consistently with skew angle. The tests typically showed a reduction in the passive force to a residual value at a normalized displacement of 0.04H to 0.06H. This post-peak reduction in passive force to a residual value is consistent with the stress-strain behavior expected from dense compacted sand and the results of the direct shear tests. Dense sands dilate during shearing and the resulting lower density leads to a reduced strength. The post-peak residual strength ranged from 53 to 72% of the peak value with an average of 60% and may be important for large displacement applications. The post-peak drop in passive force appeared to become somewhat more abrupt as the skew angle increased. The decrease in passive force is likely to be less significant for higher abutment walls as increased confinement reduces the potential for dilation during shearing.

The peak passive force for each test at a given skew angle has been divided by the peak passive force at zero skew and the results are shown as a function of skew angle in Fig. 7. As the skew angle increases, the normalized passive force decreases significantly. For example, at a skew angle of 30º the passive force is only about 50% of that with no skew. Normalized data from numerical analyses of skew abutments reported by Shamsabadi et al (2006) are also shown in Fig. 7 and the results follow the same trend line. Shamsabadi et al performed their analyses on a seat type abutment with a backwall height of the 1.68 m (5.5 ft), a width of 22.8 m (75 ft), and skew angles of 0°, 30°, 45° and 60°. The backfill consisted of silty sand with a unit weight of 18.8 kN/m^3 (120 lbs/ft^3), a cohesion of 25 kPa (500 lbs/ft^2), a soil friction angle of 34°, and a wall friction of 23° which was confined by parallel wingwalls on either side of the backwall. Analyses were performed with the Plaxis 3D finite element computer program with the Hardening Soil (HS) constitutive model (Brinkgeve 2006). The curve has been extrapolated to zero at a skew angle of 90º. As illustrated in Fig. 8, at a skew angle of 90º there would be no passive force but only transverse shear force equal to the side shear resistance on the wall. There must be a transition (Fig. 8b) from pure passive force and zero side shear for 0° skew (Fig. 8a) towards pure side shear and zero passive force at 90° skew (Fig. 8c). The side shear resistance at 90° skew would be much less than the passive force at 0° skew.

Considering the variation in backfill geometries and soil properties, the agreement in reduction factors from the numerical and physical test results is quite remarkable and suggests the potential for a simple adjustment factor to account for skew effects. However, because the correction factor produces a significant decrease in passive resistance, these large scale lab results should be verified with large scale field tests with variations in abutment geometry and possibly backfill type. Plans for additional large scale field testing are currently being developed by the authors, but in the interim, the reduction factors should be considered provisional.

As indicated previously, vertical and lateral displacement of the wall was measured during each test and the maximum values are summarized in Table 2. The displacements were typically averages of two displacements. The data in Table 2 shows that displacement was less than 4.4 mm for vertical movement and less than 2.3 mm for transverse movement for the skew angles tested.

Variation of Forces on Abutment with Skew Angle

The peak longitudinal force (P_L), peak passive force (P_P), peak transverse shear force (P_T) (computed using Eq. 2), and the peak transverse shear resistance (P_R) (computed using Eq. 3) are shown as a function of skew angle in Fig. 9. In computing P_R the wall friction was taken as 33° with cohesion of 4.5 kPa (90 psf) based on the lab test results. Although the passive force continues to decrease with skew angle, as explained previously, the longitudinal force appears to stabilize at a skew angle of 30°. Apparently, the decrease in passive resistance is partially compensated by the increased longitudinal component of the shear resistance.

Although the applied shear force increases with skew angle, the shear resistance decreases because the normal force provided by the passive force decreases. Nevertheless, as shown in Fig. 9, the applied transverse shear resistance is greater than the transverse shear force in all cases except for the 45° skew, which may explain the lack of significant transverse displacement for measured transverse force for these cases. For the 45° skew case, the transverse shear resistance is lower than the transverse shear force and transverse force was measured by the load cell. Of course, if the interface friction angle were to decrease, sliding would occur at lower skew angles.

Failure Surface Geometry

The failure surface for the no skew case was approximately the same length across the width of the sand box; however, when a skew angle was involved, the failure surface also exhibited a skew across the width of the sand box as illustrated by the photos in Fig. 10. Some edge effects appear to be present due to interface friction and geometrical variations in the plywood walls. Interface shear tests indicate that the friction angle is 15º for the plastic sheeting which could lead to errors of 3% to 6% in the measured longitudinal force assuming an average earth pressure coefficient of 4 on the sidewall. The failure surface did not manifest itself at the ground surface until after the peak force had been reached and the passive resistance had begun decreasing to the residual value.

The failure surface within the sand was clearly identifiable from the offset in the red sand columns as shown by the photo in Fig. 11. For columns closer to the wall, there was typically a lower shear offset in the column with a bent section above it and then another shear offset above the bent section. In contrast, for columns further away from the wall and closer to the ground surface there was simply one shear offset in the column. Such failure patterns suggest that the soil near the wall may be compressing more than soil away from the wall in addition to shearing along the failure surface.

The failure surface geometry is shown as a function of distance behind the middle of the wall for the various skew angles in Fig. 12. In addition, the ground surface heave is also plotted for each test. The average length of the failure surface behind the middle of the wall was 2.1 m (7.0 ft) with a standard deviation of 0.3 m (1.0 ft). The length of the failure surface ranged from 1.8 to 2.6 m (5.9 to 8.6 ft). The failure surface typically extended 75 mm to 300 mm. horizontally from the bottom of the wall then exhibited a relatively linear trend line upward to the surface. The angle of inclination of the trend line was between 19º and 21.5º with an average of 20°. Assuming that the angle of inclination (α) of the straight line segment of the log-spiral failure wedge is given by the equation

$$\alpha = 45 - \phi'/2 \tag{8}$$

as suggested by Terzaghi and Peck (1948), then the interpreted drained friction angle would be between 47º and 52º with an average of 50º. The inferred friction angle value is higher than the measured friction angle from the direct shear test, but is close the value that would be expected for the plane strain friction angle. The conditions and geometry of the sand box simulated a plane strain condition as well. Based on a number of studies, Kulhawy and Mayne (1990) determined that the plane strain friction angle for dense sand was 11% higher than the triaxial value on average. Thus, the plane strain friction angle for the sand used in the tests would be about 51°, which is approximately the same value as that of the inferred friction angle from the inclination of the failure wedge.

The heave of the failure wedge was typically about 25 mm (1.0 in) which represents a 4% heave relative to the maximum thickness of the failure wedge (0.62 m). The heave was relatively uniform along the length of the failure wedge although somewhat higher near the wall.

Displacement and Strain within the Failure Wedge

The normalized longitudinal ground surface displacements as a function of distance behind the wall are shown in Fig. 13 at the peak passive force for the tests at the four skew angles; displacement is normalized by the maximum displacement of the wall. No trends were observed with skew angle. Based on this data, the average compressive strain was computed as a function of distance behind the wall and is shown for an average wall displacement of 16 mm (0.62 inch) or 0.025H in Fig. 14. These results indicate that the failure “wedge” does not simply move as a block but undergoes significant compression as well. As discussed previously, compressive strain is highest in the sand directly behind the wall but decreases with distance. Compressive strains are as high as 7.5% near the wall but decrease to around 3.5% at 1 m (3.3 ft) behind the wall. This strain information is likely to be useful for calibrating numerical models in the future.

ANALYSIS OF TEST RESULTS

The passive force-deflection curves were computed using the computer programs PYCAP developed by Duncan and Mokwa (2001) and ABUT developed by Shamsabadi et al (2007). Both programs compute the ultimate passive force using the log-spiral method and use a hyperbolic curve which is asymptotic to the ultimate passive force to define the force-deflection curve. In defining the hyperbolic curve, Duncan and Mokwa make use of the initial elastic modulus (E) and normalized wall movement at failure, while Shamsabadi et al use the strain at 50% of the ultimate force (ε_{50}).

Because of the plane strain geometry involved in the tests, the friction angle measured in the direct shear test for triaxial conditions (ϕ'=46º) was increased to the plane strain (ϕ'_{PS}=50º) value based on the failure plane geometry and recommendations by Kulhawy and Mayne (1990). The apparent soil cohesion was taken as 4 kPa (80 psf) based on in-situ matric suction measurements in the fill with dielectric sensors and the wall friction angle was taken as 33º based on interface tests. The average moist unit weight was taken as 18.85 kN/m^3 (120.0 lb/ft^3) based on the nuclear dry density results and the post-testing moisture contents.

For the PYCAP analysis initial estimates of the soil elastic modulus (E) were made based on a range recommended by Duncan and Mokwa (2001) for dense compacted sand (E=28.8 to 57.5 MPa [600 to 1200 ksf]), but were adjusted by trial and error to a value of 48 MPa (1000 ksf) to obtain improved agreement with the measured curve shape. The back-calculated value is above the middle of the range. The normalized displacement at failure was taken as 0.03H based on the test results which is within the range recommended by Cole and Rollins (2006) and Caltrans (2001) (0.03H to 0.05H).

For the ABUT analysis initial estimates of the ε_{50} were made based on the range of recommended values (0.002 to 0.003) provided by Shamsabadi et al (2007); however, this value had to be adjusted by trial and error to a value of 0.004 to improve agreement with the measured curve shape. The cohesion was also increased slightly to 6.2 kPa (130 psf) to improve agreement. All other parameters were the same as those indicated previously.

The measured and computed passive force-deflection curves for the no skew case are shown in Fig. 15. The agreement between the measured curves and the two computed curves is very good up to the peak; however, neither method accounts for the post-peak decrease in passive. Using the measured residual friction angle in the analysis also failed to match the residual passive force in this case.

It should be noted that the computed passive force is very sensitive to variations in the soil friction angle and wall friction. Variations of ± 1° in soil friction angle produced a ± 10% change in passive force, while variations of ± 5° in the wall friction resulted in a ± 15% change in passive force. It should also be noted that for the relatively shallow depth of soil involved in the tests conducted and for many bridge abutments, the apparent cohesion used in the analysis is a particularly important parameter. For example, the apparent cohesion in this case accounts for approximately 26% of the computed passive force. For higher abutment walls, the contribution of cohesion to the overall resistance would tend to decrease somewhat as the frictional component increased due to higher confining pressure. For example, for a 2.43 m (8 ft) high backwall with the same backfill properties, apparent cohesion would only account for 9% of the total resistance. In design applications, the contribution from apparent cohesion is often neglected which would lead to an underestimate of the actual passive force. An accurate assessment of apparent cohesion could be particularly important for determining the passive force on a bridge abutment under field conditions. Matric suction measurements can be particularly helpful in this regard.

The passive force for a given skew angle ($P_{p\text{-}skew}$) can be obtained using the equation

$$P_{p\text{-}skew} = P_p \, R_{skew} \tag{8}$$

where R_{skew} is a reduction factor based on the test results shown in Fig. 7 and P_p is the passive force for the no skew case. In all cases, the width of the backwall is taken equal to the width of the backwall based on the projected area (zero skew case) rather than the actual area along the skew. Based on the limited data presently available, R_{skew} can be computed using the equation

$$R_{skew} = 7.79x10^{-5}\theta^2 - 0.018\theta + 1.0 \quad (9)$$

where θ is the abutment skew angle in degrees. It may be that the reduction factor will be dependent on geometric factors such as the width and height of the abutment wall or on differences in soil properties of the backfill. Therefore, large scale field tests are currently being performed in connection with calibrated numerical modeling to provide additional guidance to bridge design engineers.

CONCLUSIONS

1. Large scale laboratory tests and numerical analyses indicate that the peak passive force for a skewed abutment decreases significantly as the skew angle increases. Based on available results, the reduction in passive force can be accounted for by using a simple reduction factor. However, the reduction may be dependent on abutment geometry and other unknown factors. Therefore, additional large scale tests and calibrated numerical analyses would be desirable to validate the proposed reduction values and to provide additional guidance to designers.
2. For the dense compacted sand typical of approach fills for bridges, the peak passive force for both skewed and non skewed tests typically developed at longitudinal deflections between 0.025 and 0.035 times the wall height, H. However, the shape of the passive force-deflection curve up to the peak value transitioned from a typical hyperbolic shape for the no skew case to a more bi-linear shape with a relatively flat slope leading to the peak for tests involving skews

3. At wall displacements beyond the peak (0.04 to 0.06H) the passive force decreased substantially and the residual force was typically about 40% below the peak force, which is in agreement with the behavior in the direct shear tests. As the skew angle increased, the reduction in passive force appeared to be more abrupt than for the no skew cases.
4. The transverse shear resistance on the backwall of the “abutment” exceeded the applied transverse force for skew angles less than about 33°. For greater skew angles, the transverse force exceeded the shear resistance, and greater transverse load was measured by the load cell. However, transverse displacement overall was relatively minor (< 2.3 mm).
5. Using measured soil properties such as moist unit weight, plane strain soil friction angle, apparent soil cohesion, and wall friction, two computer models based on the log-spiral approach were used successfully in computing a peak passive force that was comparable to the measured force for the no skew case. However, for skewed abutments it was necessary to use a reduction factor to compute a passive force comparable to the measured value.
6. An accurate assessment of the measured passive force for the partially saturated backfill required the determination of the apparent cohesion provided by the suction in the sand. This apparent cohesion accounted for a significant percentage (26%) of the computed passive force for the 0.6 m wall, but this contribution would decrease to 9% for a 2.4 m wall.
7. The failure “wedge” did not simply move as a rigid block. Significant compressive strains (7.5%) occurred within the failure mass near the wall which decreased with distance from the wall.

REFERENCES

AASHTO (2011), Guide Specifications for LRFD Seismic Bridge Design, 2nd Edition. 286 p.

Apirakvorapinit, P., Mohammadi, J. and Shen, J. (2012). “Analytical investigation of potential seismic damage to a skewed bridge.” Practice Periodical on Structural Design and Construction, Vol. 16, No. 1, pp. 5-12

Brinkgeve, R.B.J. (2006). Plaxis 3D Tunnel, Tutorial manual, Version 2. Plaxis, Inc.

Burke, M.P. Jr. (1994). “Semi-Integral bridges: movements and forces”. Transportation Research Record 1460, Transportation Research Board, Washington, D.C., p. 1-7.

Caltrans (2001). “Seismic design criteria version 1.2.” *California Department of Transportation, Sacramento, California.*

Cole, R.T and Rollins, K.M. (2006). “Passive Earth Pressure Mobilization During Cyclic Loading.” *J. Geotech.& Geoenviron. Eng*, ASCE, 132(9), 1154-1164.

Duncan, J. M., and Mokwa, R. M. (2001). "Passive earth pressures: theories and tests." *J. Geotech. & Geoenv.l Engrg.*, ASCE Vol. 127, No. 3, pp. 248-257.

Elnashai, A.S., Gencturk, B., Kwon, O., Al-Qadi, I.L., Hashash, Y., Roesler, J.R., Kim, S.J., Jeong, S., Dukes, J., and Valdivia, A. (2010). “The Maule (Chile) Earthquake of February 27, 2010: Consequence Assessment and Case Studies.” Mid-America Earthquake Center Report No. 10-04, 190 p.

Kulhawy, F. H., and Mayne, P. W. (1990). “Manual on estimating soil properties for foundation design.” Research Project 1493-6, EL-6800, Electric Power Research Institute. Palo Alto, California.

Lee, K.L. and Singh, A. (1971). “Relative density and relative compaction.” *J. Soil Mech. and Found. Div.*, ASCE, 97(7), 1049-1052.

Lemnitzer, A., Ahlberg, E.R., Nigbor, R.L., Shamsabadi, A., Wallace, J.W., and Stewart, J.P. (2009). "Lateral performance of full-scale bridge abutment wall with granular backfill," *J. Geotech. & Geoenv. Engrg.*, ASCE, 135 (4), 506-514.

Likos, W.J. Wayllace, A., Godt, J., and Ning, L. (2010). “Direct shear apparatus for unsaturated sands at low suction and stress”. Geotech. Testing J., ASTM, 33(5)

Maroney, B.H. (1995) “Large scale abutment tests to determine stiffness and ultimate strength under seismic loading” Ph.D. Dissertation, Civil Engineering Dept., University of California, Davis.

Mokwa, R. L. and Duncan J. M. (2001). “Experimental evaluation of lateral-load resistance of Pile Caps.” *J. Geotech. & Geoenviron. Eng.*, ASCE, 127(2), 185-192.

Potyondy, J. G. (1961). "Skin friction between various souls and construction materials." *Geotechnique,* Vol. 11, No.1, pp. 339-353.

Rollins, K.M. and Cole, R.T. (2006). “Cyclic Lateral Load Behavior of a Pile Cap and Backfill.” *J. Geotech. & Geoenviron. Eng.*, ASCE, 132(9), 1143-1153.

Rollins, K.M. and Sparks, A.E. (2002) “Lateral Load Capacity of a Full-Scale Fixed-Head Pile Group.” *J. Geotech. & Geoenviron. Eng.*, ASCE, Vol. 128, No. 9, p. 711-723.

Shamsabadi, A. Kapuskar, M. and Zand, A. (2006). “Three-dimensional nonlinear finite-element soil-Abutment structure interaction model for skewed bridges”. *5^{th} National Seismic Conf. on Bridges and Highways*, FHWA, p.

Shamsabadi, A., Rollins, K.M., Kapaskur, M. (2007). “Nonlinear Soil-Abutment-Bridge Structure Interaction for Seismic Performance-Based Design.” *J. Geotech. & Geoenviron.*

Eng., ASCE, 133 (6), No. 6, 707-720.

Steinberg, E. and Sargand, S. (2010). “Thermal Expansion of Skewed Semi-Integral Bridges.” Report No. FHWA/OH-2010/16, Ohio University, Athens, OH, 87 p.200

Terzaghi K. and Peck, R. B. (1948). Soil Mechanics in Engineering Practice, John Wiley and Sons, New York, p.

Unjohn, S. (2012). “Repair and retrofit of bridges damaged by the 2010 Chile Maule Earthquake.” Procs. Intl. Symp. on Engrg. Lessons Learned from the 2011 Great East Japan Earthquake, March 1-4, Tokyo, Japan.

ACKNOWLEDGEMENTS

Funding for this study was provided by an FHWA pooled fund study supported by Departments of Transportation from the states of California, Montana, New York, Oregon, and Utah. Utah served as the lead agency with David Stevens as the project manager. This support is gratefully acknowledged; however, the opinions, conclusions and recommendations in this paper do not necessarily represent those of the sponsoring organizations.

Figure Captions

Fig. 1: Typical distribution of forces on a bridge with a skewed abutment.

Fig. 2: Schematic plan and elevation view drawings of the test layout for the skewed passive force deflection tests.

Fig. 3: Gradation for backfill sand relative to concrete sand gradation.

Fig. 4: Typical histogram of dry unit weight for backfill behind the test wall during the 30º skew test.

Fig. 5: Plot of moisture content versus depth for the various skew tests based on samples obtained immediately after tests.

Fig. 6: Passive force versus longitudinal deflection curves for the all the tests at various skew angles.

Fig. 7: Reduction Factor, R_{skew}, (passive force for a given skew angle normalized by passive force with no skew) plotted versus skew angle based on physical test results and numerical analyses.

Fig. 8: Illustration of transition of resistance on back wall from pure passive resistance at 0° skew to much lower side shear at 90° skew.

Fig. 9: Plot of longitudinal force (P_L), passive force (P_p), transverse shear resistance (P_R) and applied shear force (P_T) as a function of skew angle **(θ)**.

Fig. 10: Photos of failure surface geometry at the ground surface for (a) no skew and (b) 30 degree skew tests.

Fig. 11: Photograph showing failure surface geometry determination within sand based on offset in red sand columns for 30 degree skew test.

Fig 12: Failure surface geometry and ground surface heave as a function of distance behind the wall for tests at various skew angles.

Fig. 13: Plots of longitudinal ground surface displacement as a function of distance behind the wall for various skew angles.

Fig. 14: Average compressive strain as a function of distance behind the wall based on ground surface displacement measurements for all tests.

Fig. 15: Comparison of measured and computed passive force versus longitudinal deflection curves for the no skew case.

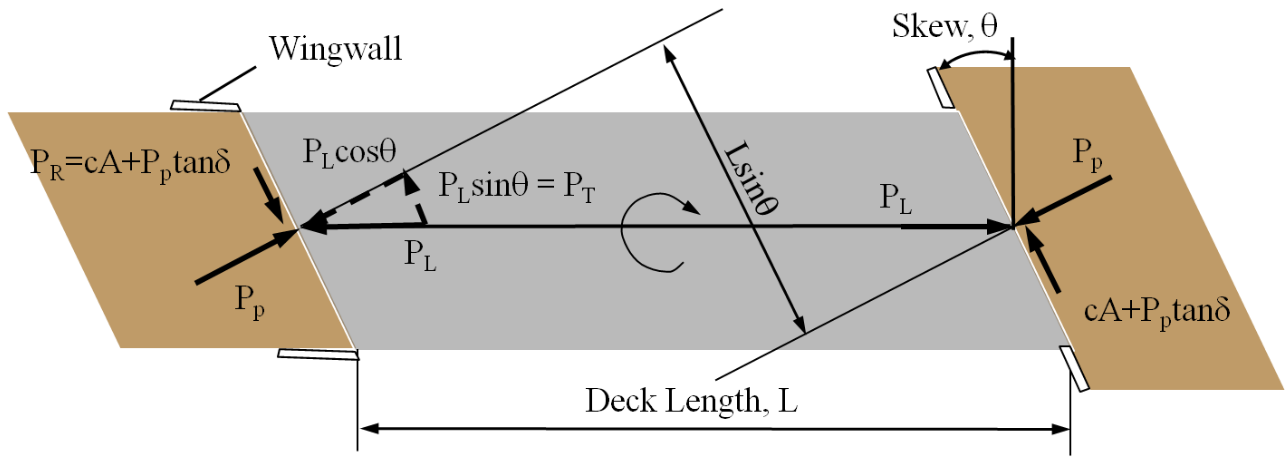

Fig. 1: Typical distribution of forces on a bridge with a skewed abutment.

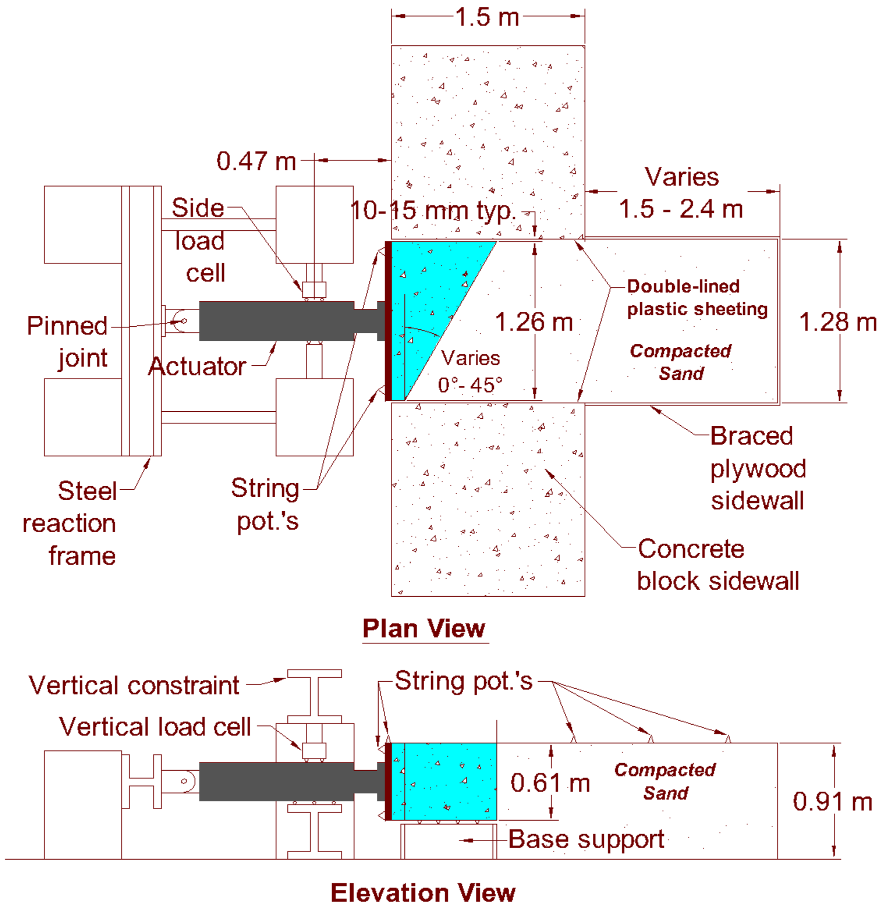

Fig. 2: Schematic plan and elevation view drawings of the test layout for the skewed passive force deflection tests.

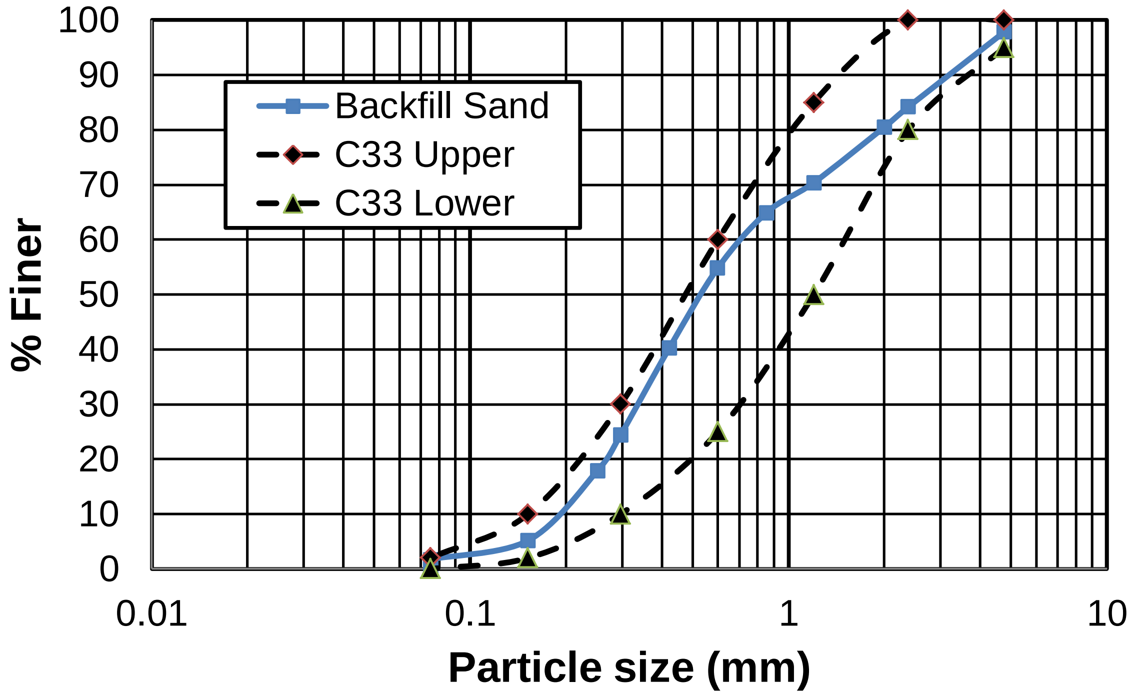

Fig. 3: Gradation for backfill sand relative to concrete sand gradation.

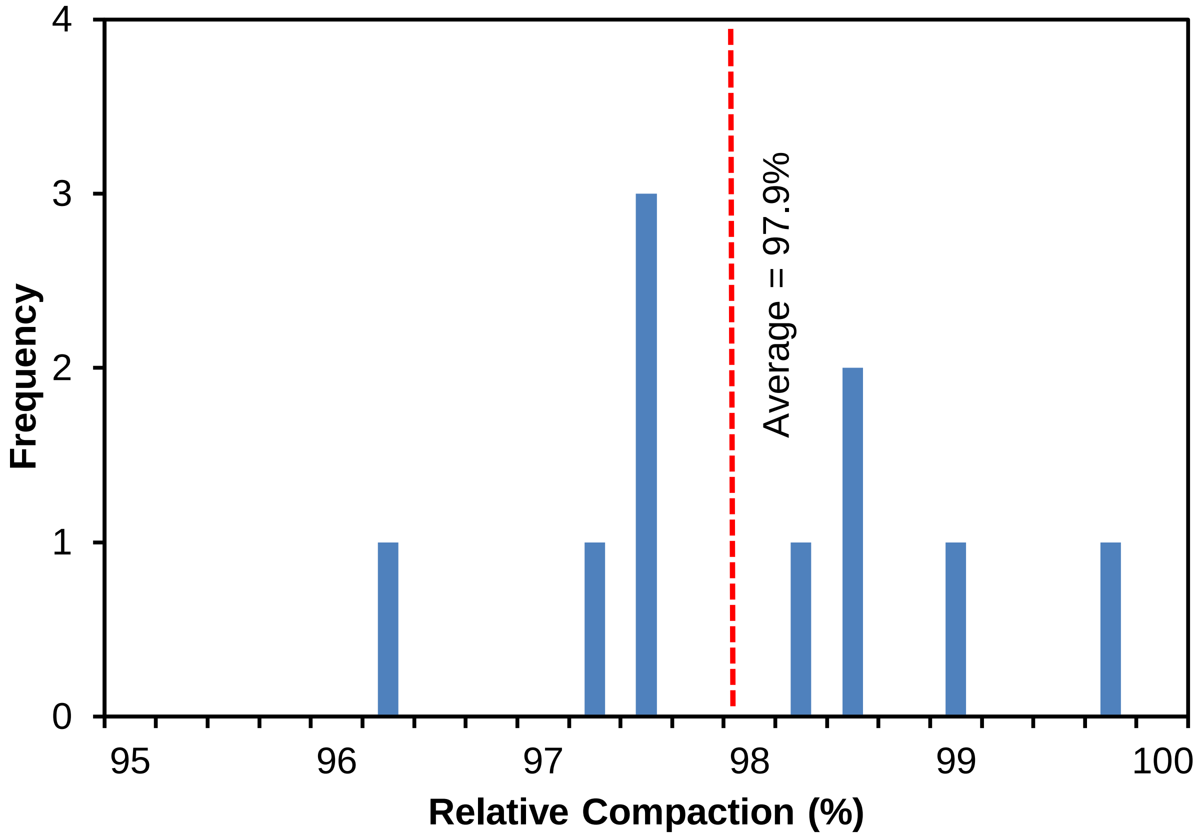

Fig. 4: Typical histogram of dry unit weight for backfill behind the test wall during the 30º skew test.

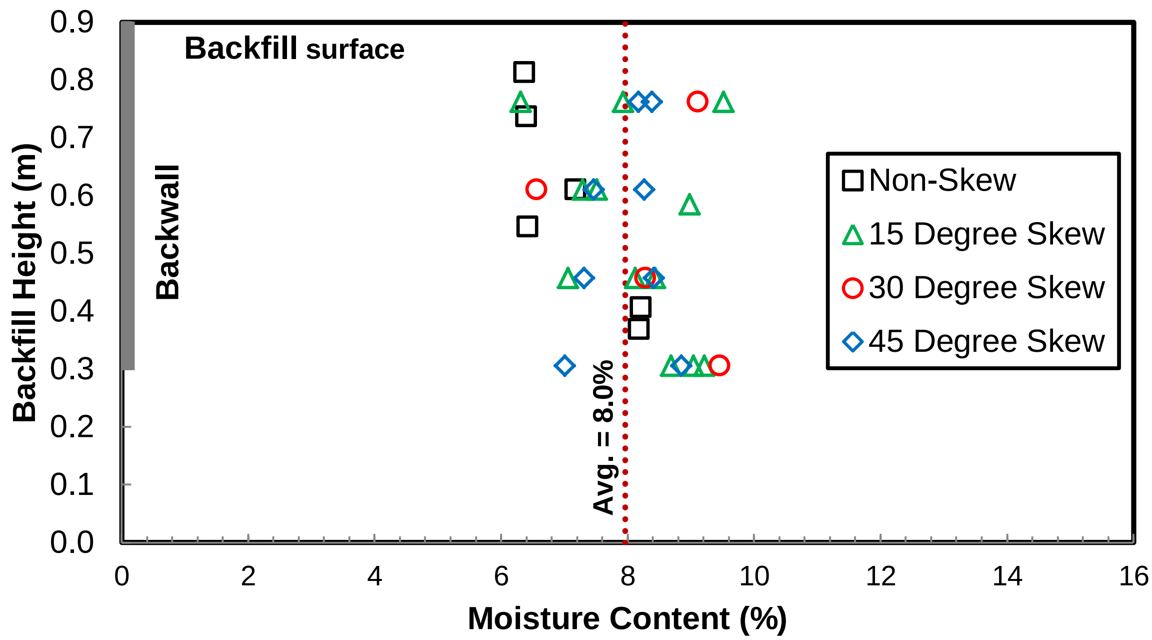

Fig. 5: Plot of moisture content versus depth for the various skew tests based on samples obtained immediately after tests.

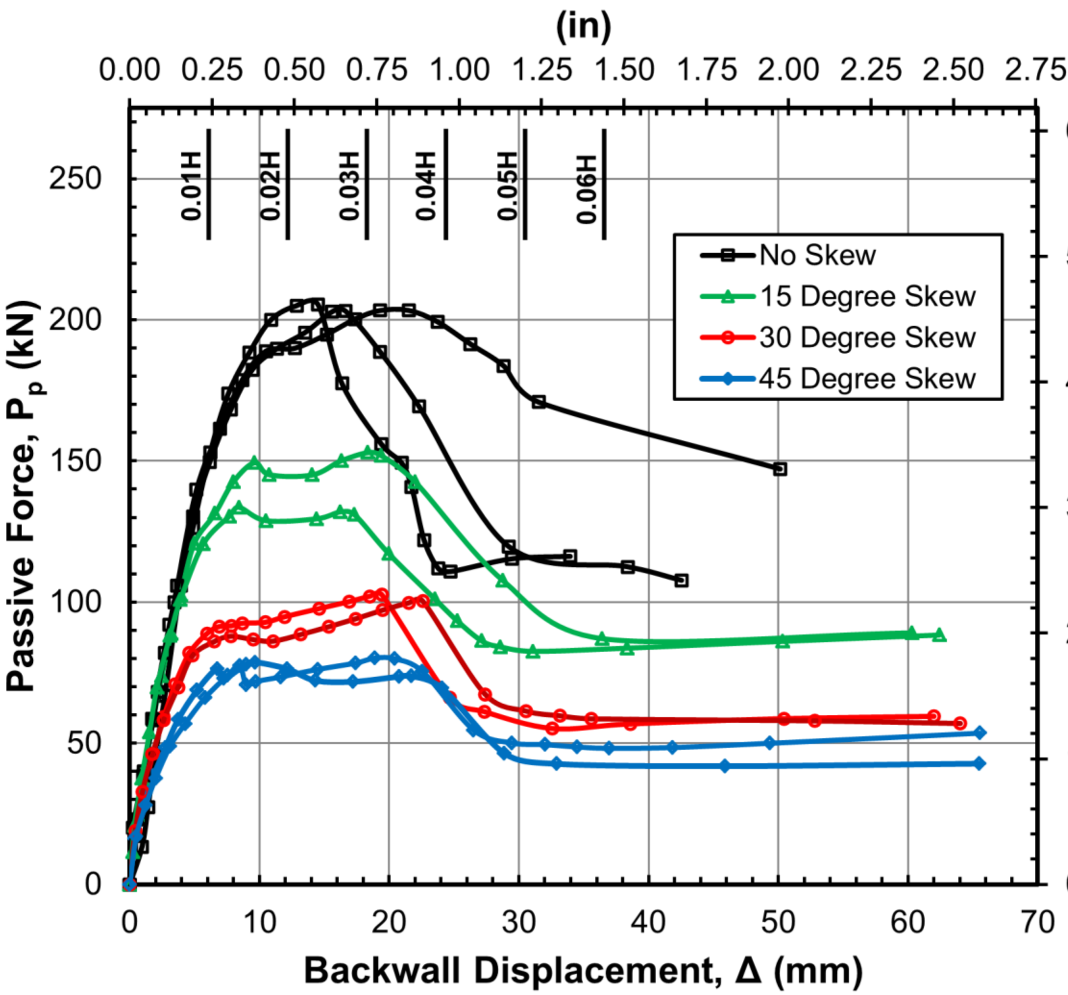

Fig. 6: Passive force versus longitudinal deflection curves for all the tests at various skew angles.

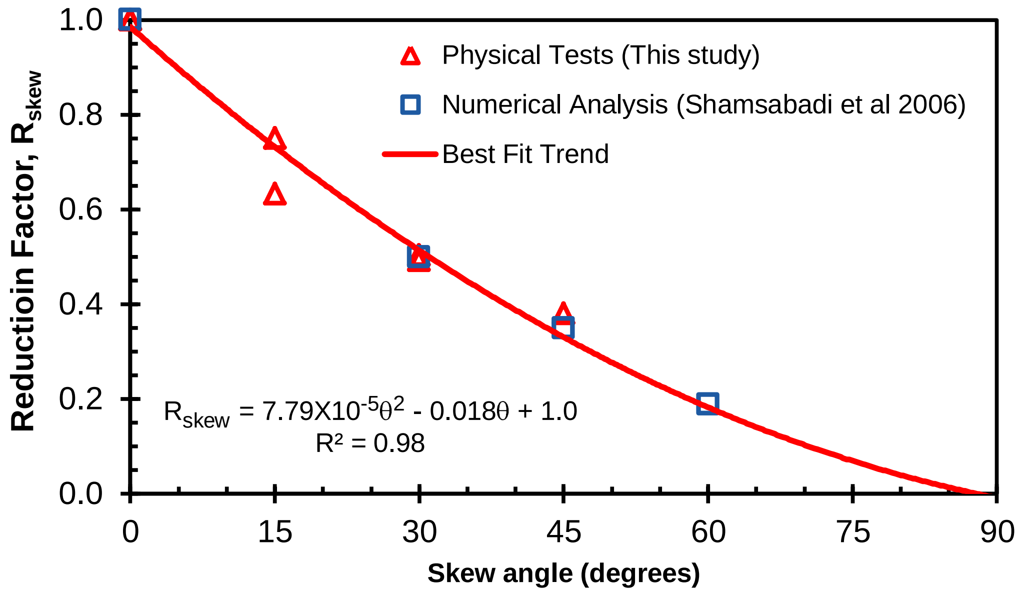

Fig. 7: Provisional reduction Factor, R_{skew}, (passive force for a given skew angle normalized by passive force with no skew) plotted versus skew angle based on physical test results and numerical analyses.

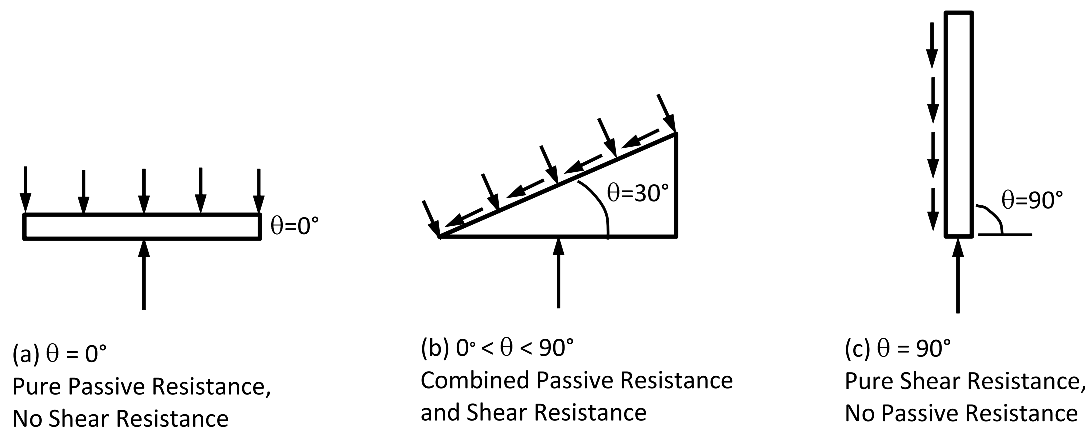

Fig. 8: Illustration of transition of resistance on back wall from pure passive resistance at 0° skew to much lower side shear at 90° skew.

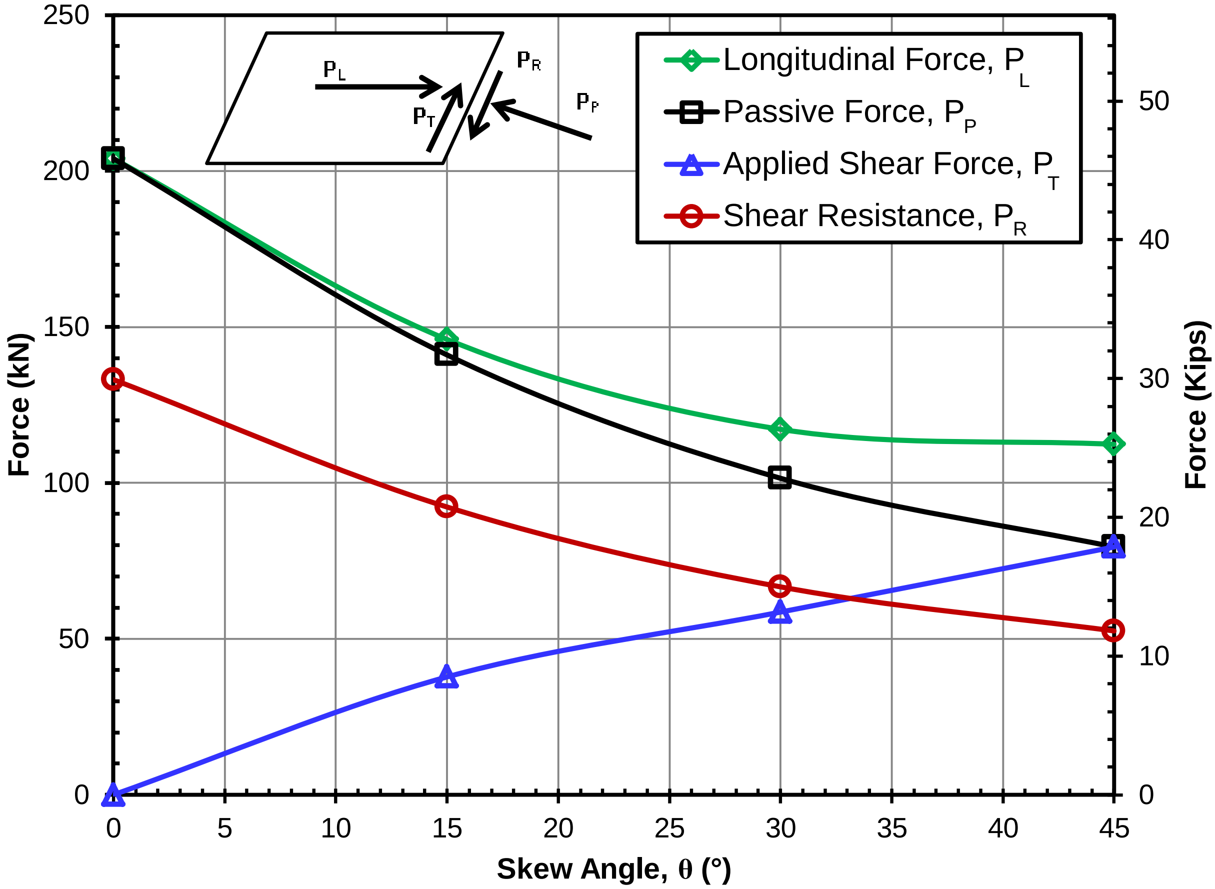

Fig. 9: Plot of longitudinal force (P_L), passive force (P_p), transverse shear resistance (P_R) and applied shear force (P_T) as a function of skew angle (θ).

(a)

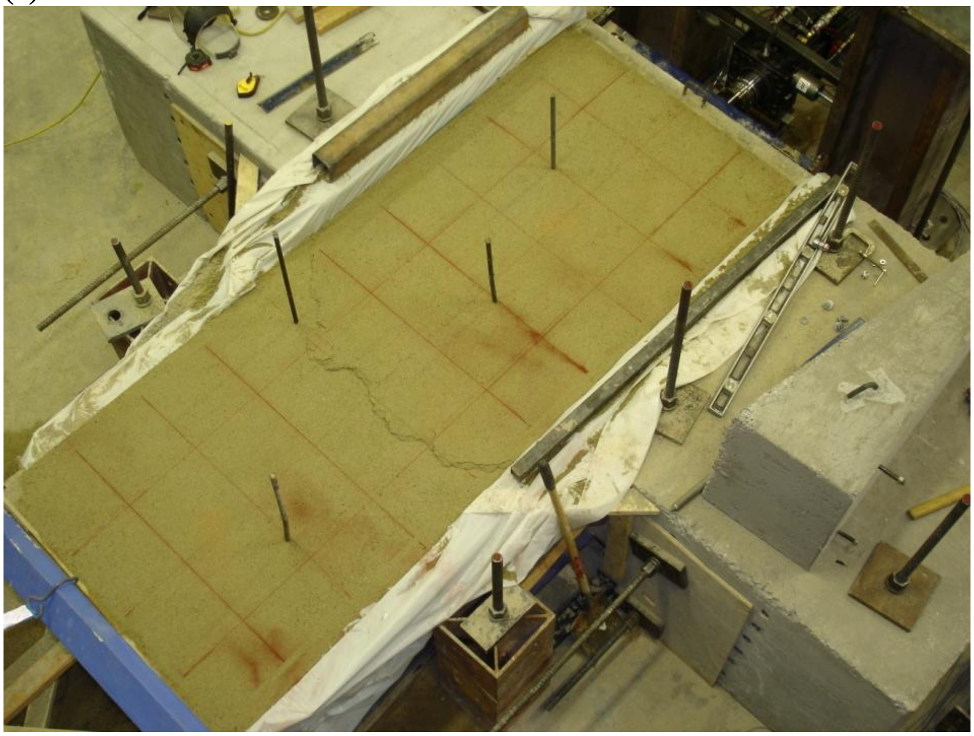

(b)

Fig. 10: Photos of failure surface geometry at the ground surface for (a) no skew and (b) 30 degree skew tests.

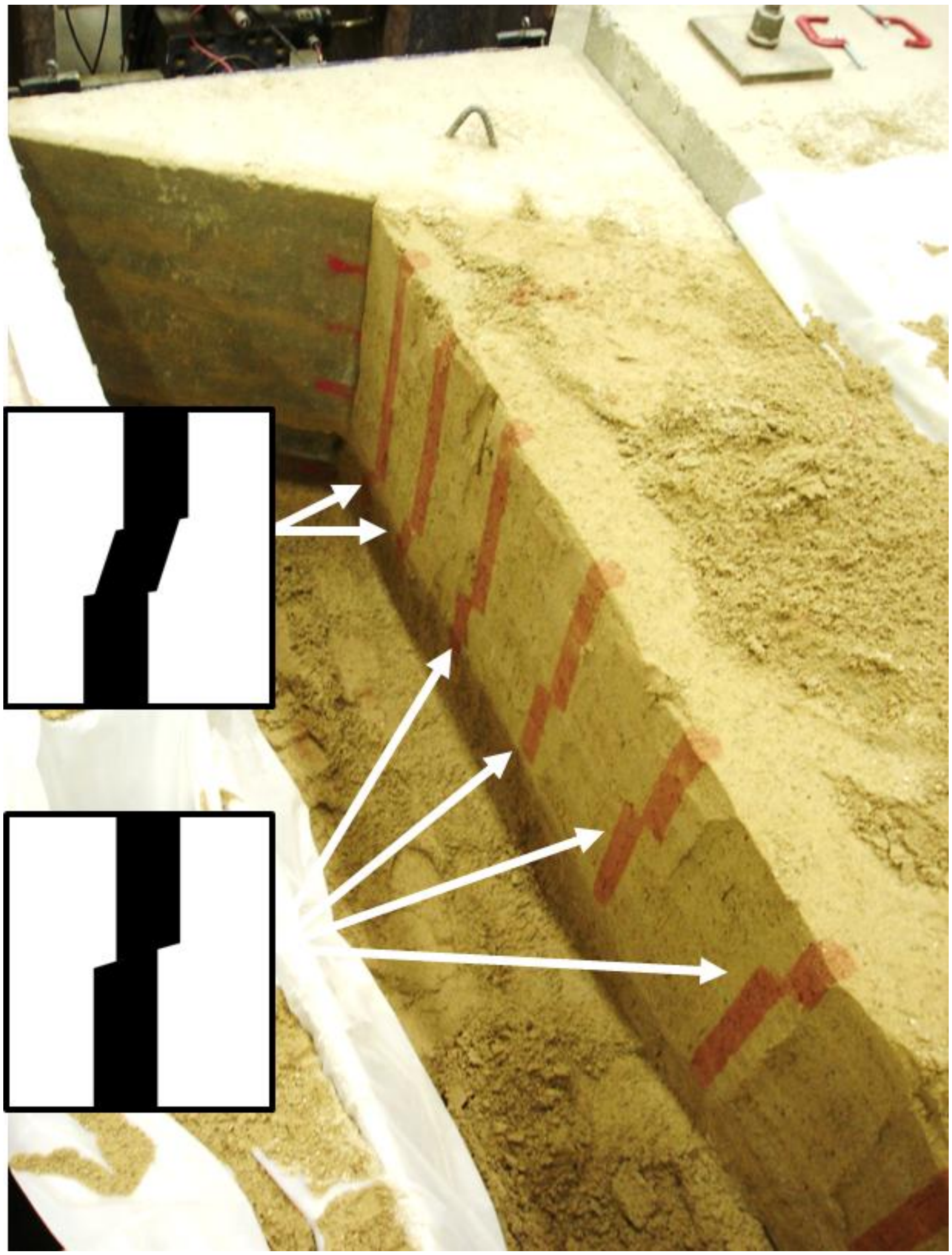

Fig. 11: Photograph showing failure surface geometry determination within sand based on offset in red sand columns for 30 degree skew test.

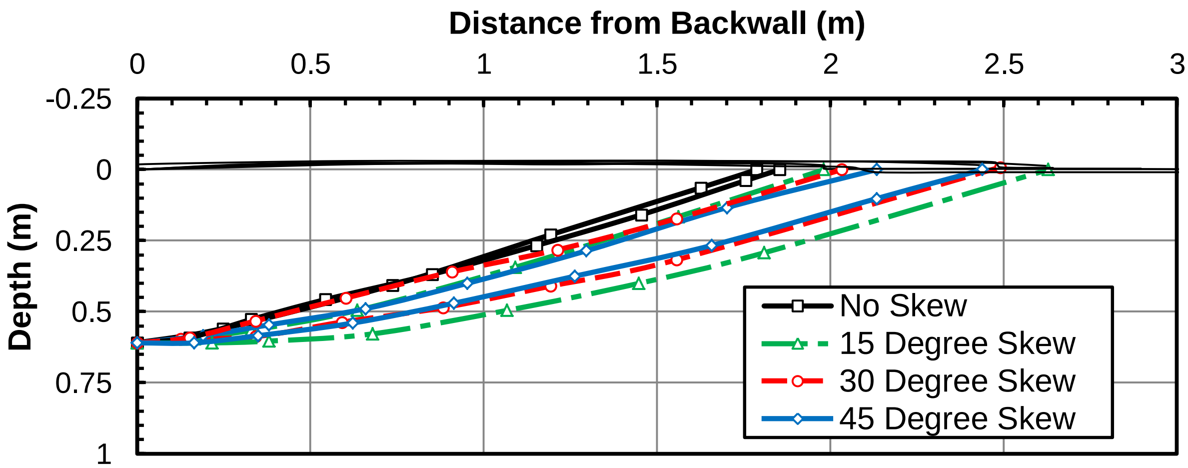

Fig 12: Failure surface geometry and ground surface heave as a function of distance behind the wall for tests at various skew angles.

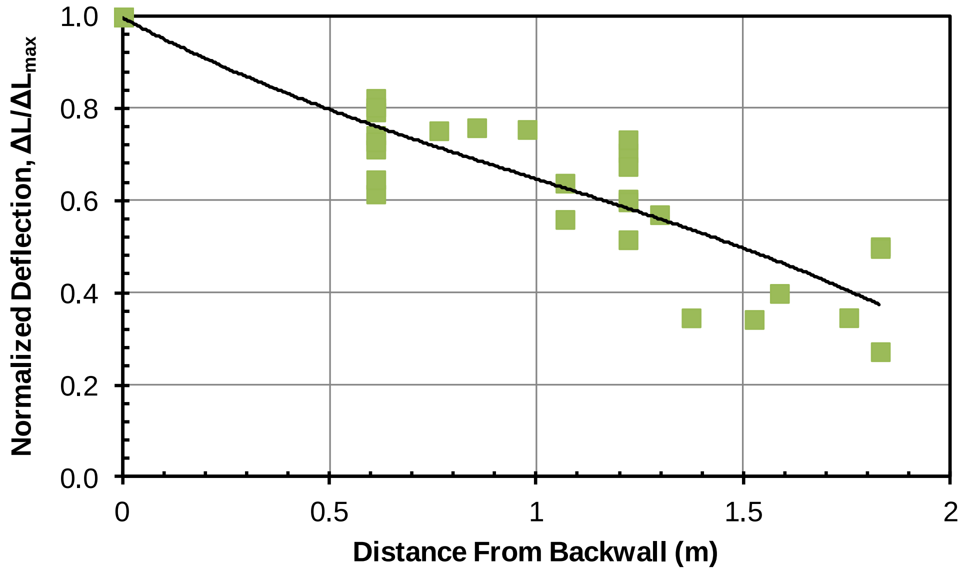

Fig. 13: Plots of longitudinal ground surface displacement as a function of distance behind the wall for various skew angles.

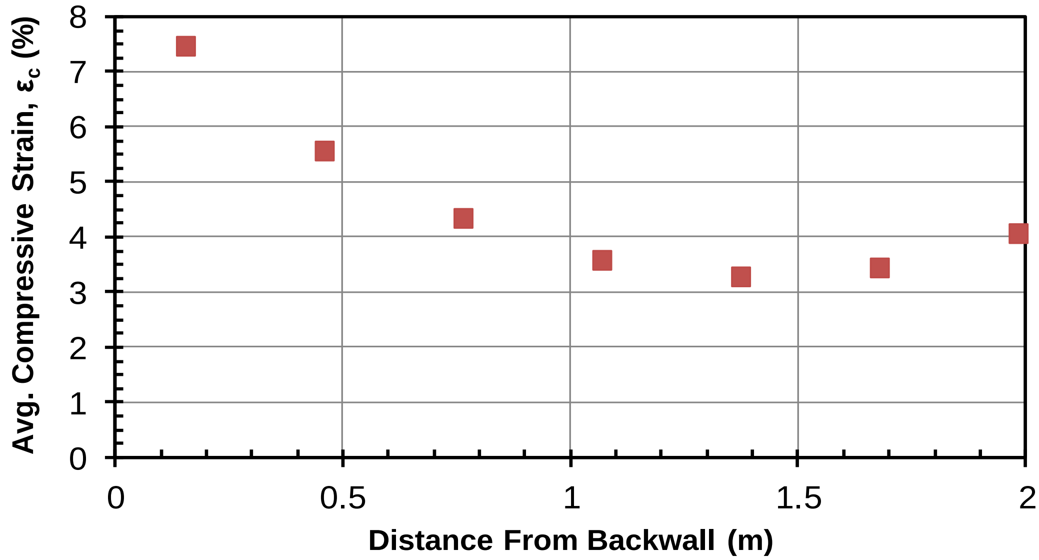

Fig. 14: Average compressive strain as a function of distance behind the wall based on ground surface displacement measurements for all tests.

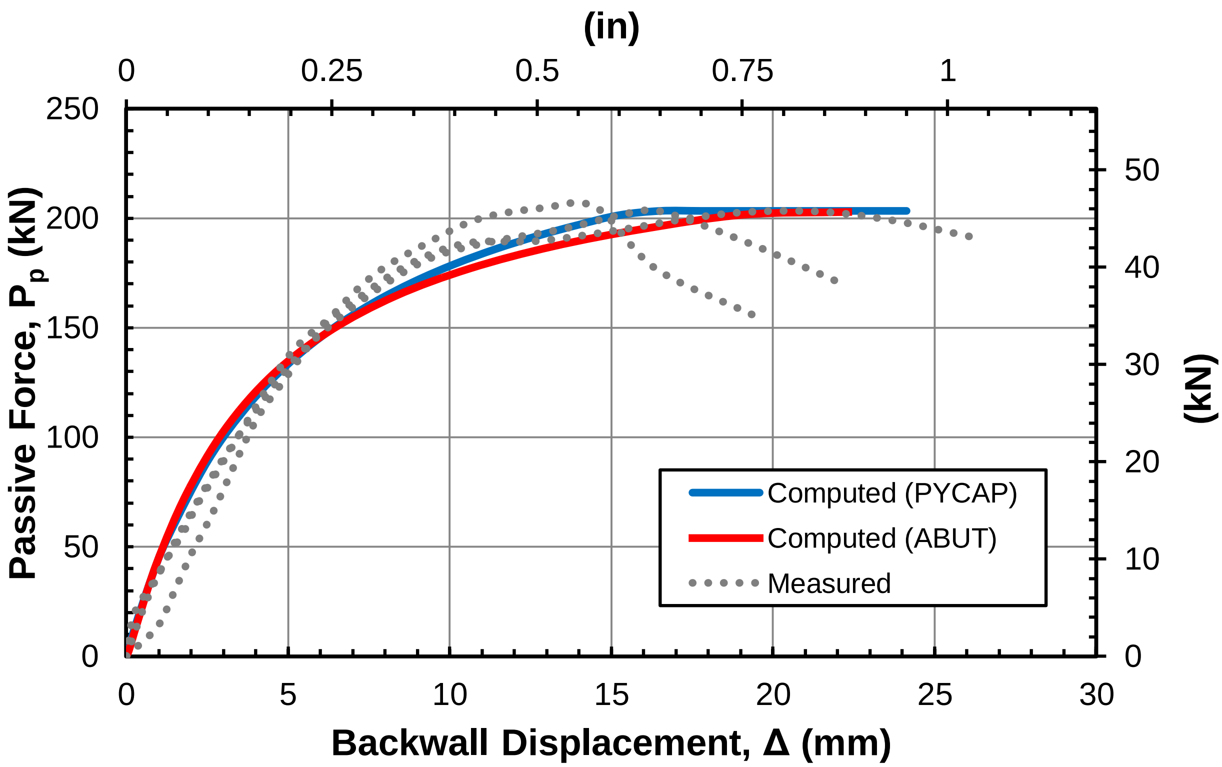

Fig. 15: Comparison of measured and computed passive force versus longitudinal deflection curves for the no skew case.

Table 1. Summary of relative compaction and average water content at time of test.

Skew Angle, θ (°)	Relative Compaction (%) Mean	Water Content (%) Mean
0	98.2	7.5
15	97.8	8.2
30	97.9	8.2
45	97.2	8.0
Overall	**97.9**	**8.0**

Table 2. Summary of the maximum vertical and transverse displacement of the wall for each test.

Backwall Movement (mm)		
Test	Vertical Disp.	Transverse Disp.
No Skew	1.5	-
No Skew	2.0	-
15°	3.4	1.3
15°	4.4	1.4
30°	0.02	2.1
30°	2.0	2.3
45°	1.4	1.8
45°	1.3	1.8
max:	**4.4**	**2.3**